Lithiation induced corrosive fracture in defective carbon nanotubes

Xu Huang, Hui Yang, Wentao Liang, Muralikrishna Raju, Mauricio Terrones et al.

Additional information on Appl. Phys. Lett.

Lithiation induced corrosive fracture in defective carbon nanotubes

Xu Huang,[1] Hui Yang,[1] Wentao Liang,[1] Muralikrishna Raju,[2] Mauricio Terrones,[3] Vincent H. Crespi,[3] Adri C. T. van Duin,[2] and Sulin Zhang[1,a)]

[1]*Department of Engineering Science and Mechanics, Pennsylvania State University, University Park, Pennsylvania 16802, USA*
[2]*Department of Mechanical and Nuclear Engineering, Pennsylvania State University, University Park, Pennsylvania 16802, USA*
[3]*Department of Physics, Pennsylvania State University, University Park, Pennsylvania 16802, USA*

We perform molecular dynamics simulations to elucidate lithiation induced fracture mechanisms of defective single-walled carbon nanotubes (SWCNTs). Our simulations reveal that variations of defect size and lithium concentration set two distinct fracture modes of the SWCNTs upon uniaxial stretch: abrupt and retarded fracture. Abrupt fracture either involves spontaneous lithium weakening of the propagating crack tip or is absent of lithium participation, while retarded fracture features a "wait-and-go" crack extension process in which the crack tip periodically arrests and waits to be weakened by diffusing lithium before extension resumes. Our study sheds light on the rational design of high-performance CNT-based electrodes. © *2013 AIP Publishing LLC*. [http://dx.doi.org/10.1063/1.4824418]

Carbon nanotube (CNT) is being considered as one of the high-power and high-energy electrode materials in advanced lithium (Li) ion batteries (LIBs) due to its superior electrical conductivity and high surface area as compared to the bulk graphite.[1–6] Because of their excellent mechanical flexibility and extremely high fracture strength, CNTs have also been expected to possess longer cycle life than the conventional carbonaceous materials.[7–9] However, our recent *in-situ* transmission electron microscopy (TEM) studies evidenced that lithiation drastically embrittles multi-walled CNTs (MWCNTs), manifested by the sharp fracture edges as well as apparently low fracture strain,[10] opposite to the highly reversible deformability of pristine CNTs.[11,12] The drastic embrittlement motivated an important question as to whether defects would pre-exist in the MWCNTs of the experiments or nucleate during the experimentation, and what roles these defects might play in the embrittlement of the lithiated CNTs.

Defects are known to influence the performance of CNT-based electrodes in several aspects. For a pristine MWCNT, diffusion of Li from its open ends to its center constitutes the only channel for Li intercalation into the interfacial spacings of the MWCNT.[13–16] A long, pristine MWCNT thus may have less competitive charging/discharging rates due to the long diffusion distance. The presence of defects may enhance the charging/discharging rates of MWCNTs since Li may be able to diffuse through the defects, a shortcut to the center of the MWCNTs.[17–22] In addition, the presence of a defect generates a local stress field around it, which may create a chemical potential gradient that drives Li diffusion toward the defect.[23,24] The aggregated Li subsequently weakens the C-C bonds around the defect, acting as a corrosive agent that modulates crack nucleation and propagation.[24,25] Such a

complicated interplay between defects and Li diffusion has remained elusive and merits a detailed study.

In this Letter, we perform molecular dynamics (MD) simulations with the ReaxFF reactive force field[24,26,27] to uncover the lithiation-mediated corrosive failure mechanisms in defective single-walled CNTs (SWCNTs). The ReaxFF combines a bond-distance/bond-order relationship with a geometry-dependent charge calculation, and provides a highly transferable method, applicable to covalent, metallic, and ionic materials and their interfaces.[26,28] The ReaxFF generally fits not only thermodynamic properties but also kinetic properties, including reaction and diffusion barriers, both from first-principles based simulations. The ReaxFF has been adequately shown to provide an accurate account of the chemo-mechanical behavior of the Li/C systems, while computationally much more efficient than first-principles simulations.[24,28]

To study the effect of defect size, we choose two representative types of defects in a (18, 0) zigzag SWCNT: a single vacancy and a hole-like defect created by removing 10 carbon atoms.[14,29] Mechanical degradation by both types of defects has been widely studied in the previous research.[30–33] In our MD simulations, periodic boundary condition is applied in the axial direction of the SWCNT. The length of the CNT is 7.2 nm (∼1200 carbon atoms in total). Li atoms are randomly added to the outer surface of the SWCNT with varying concentrations, as shown in Fig. 1. Prior to loading, the system is dynamically equilibrated to its lowest energy state. Thereafter, the SWCNT is uniaxially stretched at a constant stretching rate of 0.01 Å/ps until the SWCNT breaks into two pieces. Throughout the simulations, the system temperature is maintained at 300 K using the Nosé-Hoover thermostat.

Figure 1 depicts the fracture process of the SWCNTs with the two types of defects at four different Li concentrations: Li:C = 0, 1:36, 1:12, and 1:6. Zero Li concentration corresponds to the pure carbon structure. Upon uniaxial

---

a)Author to whom correspondence should be addressed. Electronic mail: suz10@psu.edu

(A) Hole

(B) SV
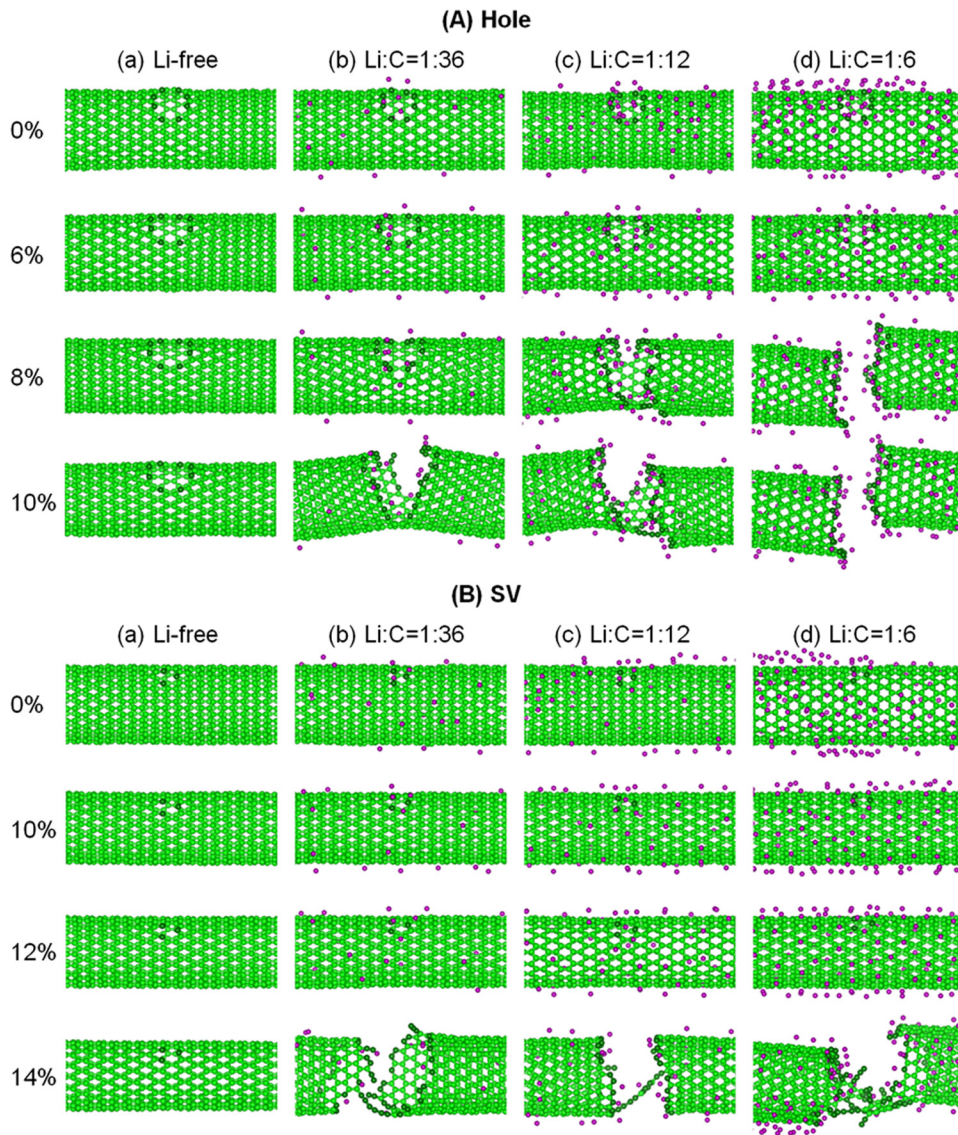
FIG. 1. Fracture of defective (18, 0) SWCNTs with varying Li concentrations (green: carbon; purple: Li, dark green: carbon atoms constitute the defects or the cracked surfaces) containing two types of defects: hole-like defect (panel A) and single vacancy (panel B). Four subfigures of each column in each panel present the snapshots in the fracture process at applied tensile strain (listed on the left) and specified Li concentrations (listed on the top). For both types of defects, Li tends to aggregate around the defect before crack nucleates, weakening the C-C bonds around the defect, leading to reduced fracture strength. The defect size and Li concentration set two distinct fracture modes: abrupt fracture (panel A: (a) and (d); panel B: (a)–(d)) and retarded fracture (panel A: (b) and (c)), differentiated by the crack propagation speed.

stretch of the SWCNTs, Li tends to aggregate around the defects before fracture initiates, driven by the chemical potential difference from anywhere else to the vicinity of the defects. For the hole-like defect, some Li atoms even reach the inner surface of the CNT via through-role diffusion.[14,29] Such through-defect diffusion is less likely for the single-vacancy defects because of larger diffusion barrier. The dynamic Li redistribution via diffusion will be further discussed later. The aggregated Li atoms weaken the C-C bonds around the defects. The number of Li atoms aggregated around the defects depends on the Li concentration, leading to the different levels of weakening.[24] For this reason, the fracture strength of the SWCNTs monotonically decreases with increasing Li concentration for both types of defects, as listed in Table I. The weakening effect of Li atoms is stronger in the hole-like defect than in the single-vacancy defect since the hole-like defect can accommodate more Li atoms around it. The presence of Li atoms not only weakens the defects but also softens the tubes,[34] leading to a complicated dependence of the onset fracture strain (the critical applied strain at which crack nucleates) on the Li concentration. Our simulations show that for both types of defects the onset fracture strain decreases when the Li concentration increases

from 0 to 1:12, and then increases slightly at Li concentration of 1:6, as listed in Table I. For all the simulations presented above, dislocations are not observed during the fracture process, indicating that the fracture is purely brittle. We also observed the cracks propagate along an irregular fracture path rather than a straight one because of the spatial randomness of Li weakening on the fracture path.

The defect size and Li concentration not only set the fracture strength and onset fracture strain but also the

TABLE I. The onset fracture strain, rapture strain, and fracture strength of defective (18, 0) SWCNTs with varying Li concentrations (SV: single vacancy).

Defects	Li:C	Onset fracture strain (%)	Rapture strain (%)	Fracture strength (GPa)
Hole	0	14.08	14.29	107.90
Hole	1:36	7.82	10.80	49.07
Hole	1:12	7.03	15.11	44.27
Hole	1:6	7.15	7.73	43.94
SV	0	15.49	15.71	124.77
SV	1:36	12.53	12.75	88.78
SV	1:12	12.52	12.87	80.10
SV	1:6	13.55	13.78	75.13
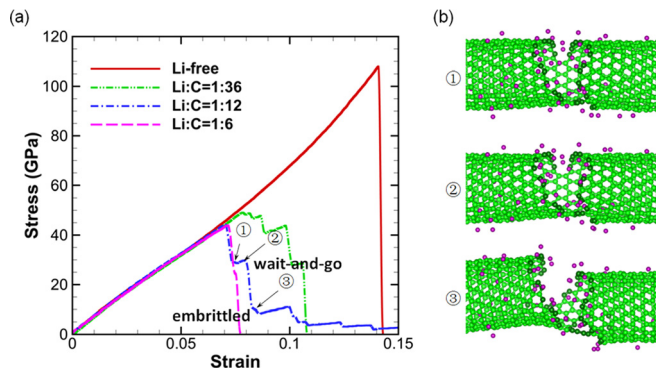
FIG. 2. (a) Stress-strain curves of the SWCNTs containing a hole-like defect. (b) Three fractural states of SWCNTs showing a "wait-and-go" fracture behavior of SWCNTs with relatively low Li concentration (for Li:C = 1:12).

FIG. 3. Active lithium diffusion on the surface of SWCNTs with a hole-like (a) and single-vacancy defect (b). For both (a) and (b), Li:C = 1:12.

fracture mode. Two typical fracture modes are observed in our simulations: abrupt fracture in which the SWCNT breaks into pieces in a very short time by fast crack propagation and retarded fracture in which considerable stretch needs to be applied beyond the onset fracture strain before complete rupture occurs. The fracture modes can be deduced from the difference between the onset fracture strain and the rupture strain at which the SWCNT breaks into pieces, as listed in Table I, with a small (considerable) difference indicating abrupt (retarded) fracture. These two fracture modes are also clearly shown in the stress-strain curves for the hole-like defect with different Li concentrations, as seen in Fig. 2(a). Abrupt fracture occurs for the Li-free and the highest Li concentration (for Li:C = 1:6) cases, manifested by a sudden drop of the stress to zero at the rupture strains; whereas for retarded fracture, the stress decreases gradually to zero over a large straining period (for Li:C = 1:12 and 1:36).

We observed that abrupt fracture occurs under two extreme conditions: spontaneous weakening by Li or in the absence of Li participation during crack nucleation and propagation. For the Li-free cases and those of single-vacancy defected SWCNTs, the high onset fracture strains correspond to large strain energy accumulated in the SWCNTs prior to crack nucleation. The sudden release of the large strain energy upon crack nucleation provides a large driving force, leading to fast crack propagation, which leaves insufficient time for Li diffusion and redistribution. As a result, Li diffusion does not participate in the facture of these cases. For the highest Li concentration of the hole-like defect, the onset fracture strain is small, so as the driving force for crack propagation. However, the highly concentrated Li spontaneously weakens the crack tip wherever it extends,[24] also leading to fast crack propagation. It should be noted that there are two co-existing weakening effects for the CNTs: the defects and the Li atoms.[10] The weakening effect due to the presence of Li atoms is more pronounced at large strains (>8%), manifested by the decreasing tangent moduli with increasing Li concentrations for the single vacancy defected CNTs. The weakening effect of the Li atoms is indistinguishable from the stress-strain curves for the hole-defected CNTs since their fracture strains are relatively small (<8%).

Retarded fracture occurs at relatively low Li concentrations (Li:C = 1:36 and 1:12) for the hole-like defect. The large defect size corresponds to a relatively small onset fracture strain, which potentially lowers the drive force for crack propagation. Crack propagation in these cases involves active Li participation, exhibiting a "wait-and-go" fracture behavior, as shown in Fig. 2 for Li:C = 1:12. At an applied strain beyond the onset of fracture, the system arrives at state ① at which the crack arrests. Further stretching the CNT results in insufficient stress buildup at the crack tip to break the crack-tip C-C bond. The crack is thus at a waiting state for Li atoms to arrive by diffusion to weaken the crack-tip bond. At state ②, new Li atoms finally arrive at the crack tip, chemically weaken the crack-tip C-C bond, and the crack propagation resumes. At state ③, the bond at the crack tip breaks, and the crack is again at the waiting state since there are no Li atoms at the new crack tip. Such a "wait-and-go" process repeats until the CNT breaks into two pieces. The "wait-and-go" fracture process results in increased stretchability and fracture toughness (indicated by the area underneath the stress-strain curve).
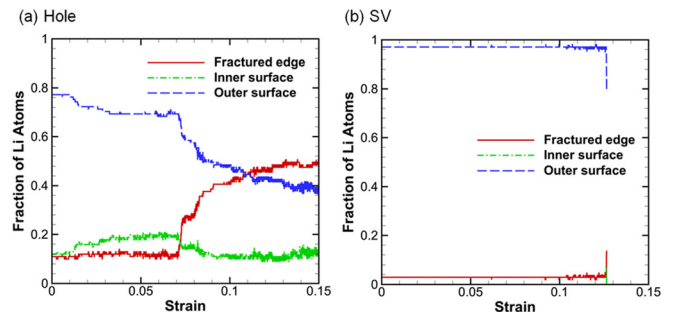
To further illustrate the active role of Li diffusion in the fracture of the SWCNTs, we plot in Fig. 3 the dynamic distribution of Li on the surface of the SWCNTs during the loading process, where the Li concentration is Li:C = 1:12. The hole-like defect (a) accommodates more Li atoms than the single-vacancy defect (b) prior to loading (red lines). Considerable Li atoms diffuse through the hole and arrive at the inner surface of the SWCNT (green line). Upon uniaxial stretch, Li atoms diffuse to the inner surface of the CNT, possibly due to the enlarged hole size and reduced crossing migration barrier for Li. As crack propagates, the spatial distribution of Li atoms changes rapidly, with significant Li atoms diffusing from the outer and inner surfaces to the newly created fractured surfaces driven by the chemical potential gradient. While for the single-vacancy defected SWCNTs, Li distribution remains nearly unchanged until complete rapture occurs.

In conclusion, our systematic MD simulations identify two distinct fracture modes, abrupt and retarded fracture, in lithiated SWCNT containing two types of defects, single-vacancy and hole-like defect. Our analysis reveals that the defect size and Li concentration set the onset fracture strain, fracture strength, as well as the crack propagation speed. We further note that the relative time scales of crack propagation and Li diffusion dictate the fracture mode. Following the same argument, varying the loading rate may also control the fracture mode of the defective CNTs, which merits more detailed study. Our failure analysis of the defective CNTs upon lithiation provides fundamental guidance to the lifetime extension of CNT-based anode materials.

[1] L. Dai, D. W. Chang, J.-B. Baek, and W. Lu, Small **8**, 1130 (2012).
[2] G. Centi and S. Perathoner, ChemSusChem **4**, 913 (2011).
[3] N. A. Kaskhedikar and J. Maier, Adv. Mater. **21**, 2664 (2009).
[4] C. de las Casas and W. Z. Li, J. Power Sources **208**, 74 (2012).
[5] B. J. Landi, C. D. Cress, and R. P. Raffaelle, J. Mater. Res. **25**, 1636 (2010).
[6] W. H. Shin, H. M. Jeong, B. G. Kim, J. K. Kang, and J. W. Choi, Nano Lett. **12**, 2283 (2012).
[7] J. Chen, A. I. Minett, Y. Liu, C. Lynam, P. Sherrell, C. Wang, and G. G. Wallace, Adv. Mater. **20**, 566 (2008).
[8] S. Y. Chew, S. H. Ng, J. Wang, P. Novák, F. Krumeich, S. L. Chou, J. Chen, and H. K. Liu, Carbon **47**, 2976 (2009).
[9] I. Lahiri, S. W. Oh, J. Y. Hwang, S. Cho, Y. K. Sun, R. Banerjee, and W. Choi, ACS Nano **4**, 3440 (2010).
[10] Y. Liu, H. Zheng, X. H. Liu, S. Huang, T. Zhu, J. Wang, A. Kushima, N. S. Hudak, X. Huang, S. Zhang, S. X. Mao, X. Qian, J. Li, and J. Y. Huang, ACS Nano **5**, 7245 (2011).
[11] B. G. Demczyk, Y. M. Wang, J. Cumings, M. Hetman, W. Han, A. Zettl, and R. O. Ritchie, Mater. Sci. Eng., A **334**, 173 (2002).
[12] J. N. Coleman, U. Khan, W. J. Blau, and Y. K. Gun'ko, Carbon **44**, 1624 (2006).
[13] H. Shimoda, B. Gao, X. P. Tang, A. Kleinhammes, L. Fleming, Y. Wu, and O. Zhou, Phys. Rev. Lett. **88**, 015502 (2002).
[14] V. Meunier, J. Kephart, C. Roland, and J. Bernholc, Phys. Rev. Lett. **88**, 075506 (2002).
[15] M. Khantha, N. A. Cordero, J. A. Alonso, M. Cawkwell, and L. A. Girifalco, Phys. Rev. B **78**, 115430 (2008).
[16] J. Sun, H. Liu, X. Chen, D. G. Evans, W. Yang, and X. Duan, Adv. Mater. **25**, 1125 (2013).
[17] H.-C. Shin, M. Liu, B. Sadanadan, and A. Rao, J. Solid State Electrochem. **8**, 908 (2004).
[18] J. Y. Eom, H. S. Kwon, J. Liu, and O. Zhou, Carbon **42**, 2589 (2004).
[19] J. Eom, D. Kim, and H. Kwon, J. Power Sources **157**, 507 (2006).
[20] S. Yang, H. Song, X. Chen, A. V. Okotrub, and L. G. Bulusheva, Electrochim. Acta **52**, 5286 (2007).
[21] C. Masarapu, V. Subramanian, H. Zhu, and B. Wei, Adv. Funct. Mater. **19**, 1008 (2009).
[22] S. Chen, W. Yeoh, Q. Liu, and G. Wang, Carbon **50**, 4557 (2012).
[23] S. S. Terdalkar, S. Huang, H. Y. Yuan, J. J. Rencis, T. Zhu, and S. L. Zhang, Chem. Phys. Lett. **494**, 218 (2010).
[24] H. Yang, X. Huang, W. Liang, A. C. T. van Duin, M. Raju, and S. Zhang, Chem. Phys. Lett. **563**, 58 (2013).
[25] R. Grantab and V. B. Shenoy, J. Electrochem. Soc. **159**, A584 (2012).
[26] A. C. T. van Duin, S. Dasgupta, F. Lorant, and W. A. Goddard, J. Phys. Chem. A **105**, 9396 (2001).
[27] X. Huang, H. Yang, A. C. T. van Duin, K. J. Hsia, and S. Zhang, Phys. Rev. B **85**, 195453 (2012).
[28] S. S. Han, A. C. T. van Duin, W. A. Goddard, and H. M. Lee, J. Phys. Chem. A **109**, 4575 (2005).
[29] K. Nishidate and M. Hasegawa, Phys. Rev. B **71**, 245418 (2005).
[30] S. L. Mielke, D. Troya, S. Zhang, J. L. Li, S. P. Xiao, R. Car, R. S. Ruoff, G. C. Schatz, and T. Belytschko, Chem. Phys. Lett. **390**, 413 (2004).
[31] M. Sammalkorpi, A. Krasheninnikov, A. Kuronen, K. Nordlund, and K. Kaski, Phys. Rev. B **70**, 245416 (2004).
[32] S. L. Zhang, S. L. Mielke, R. Khare, D. Troya, R. S. Ruoff, G. C. Schatz, and T. Belytschko, Phys. Rev. B **71**, 115403 (2005).
[33] T. Dumitrica, M. Hua, and B. I. Yakobson, Proc. Natl. Acad. Sci. U.S.A. **103**, 6105 (2006).
[34] X. H. Liu, J. W. Wang, Y. Liu, H. Zheng, A. Kushima, S. Huang, T. Zhu, S. X. Mao, J. Li, S. Zhang, W. Lu, J. M. Tour, and J. Y. Huang, Carbon **50**, 3836 (2012).